JNK, ERK and p38. We found that MC3181 was able to induce a significant reduction of P-JNK levels in the metastasis-derived melanoma cell line, starting within 30 minutes after addition of the drug (Figure 7a). This reduction persisted for 48 hours in the presence of 1 μM MC3181. Of note, when WM266.4 cells were treated with higher MC3181 concentrations (i.e. 2.0 and 4.0 μM) we observed a persistent JNK activation that paralleled an increase of apoptotic cells, as previously reported (Supplementary Figure 6) [5, 6]. Phospho-activation of p38 was also significantly affected by 1.0 μM MC3181 up to 48 hours (P-p38, Figure 7c). As regards ERK activation, the levels of P-ERK in drug treated cells were not significantly different from those of control cells, at all of the investigated MC3181 concentrations (Figure 7b).

Autophagy is not involved in the anti-metastatic effect of MC3181

As autophagy seems to be involved in tumor cell motility and invasion [12], we investigated the impact of subtoxic concentrations of MC3181 on the basal autophagy of WM266.4 cells. Western blot analysis showed that a 48-hours treatment with low concentrations of MC3181 did not significantly affect the levels of the autophagosome-associated LC3-II protein (Supplementary Figure 7). Thus, the anti-metastatic activity of MC3181 is not attributable to autophagy modulation.

MC3181 reduces the expression of proteins involved in tumor invasion and angiogenesis and increases the level of the AP2 transcription factor

Then, we checked the expression levels of several proteins involved in the extravasation process. Treatment of WM266.4 cells with 1.0 μM MC3181 caused a sustained increase of the transcription factor AP2 (activating enhancer binding protein 2), starting within 30 minutes after addition of the drug (Figure 7d and 7e). Furthermore, 1.0 μM MC3181 caused a significant and sustained decrease in the expression of the adhesion molecules MCAM/MUC18 (CD146), VEGF and N-cadherin (Figure 7d, 7f, 7g and 7h). Of note, the expression of the latter protein was significantly affected also by lower concentrations of MC3181.

MC3181 oral administration reduces melanoma-induced lung metastases

To assess the potential antimetastatic effect of MC3181 *in vivo*, B6 mice were injected i.v. with syngeneic melanoma cells at day 0, and treated 8 hours later, and subsequently on a daily base, with an oral administration of the drug. Two weeks after tumor cell injection, animals were sacrificed, lungs explanted and metastases counted. MC3181 treatment reduced by more than 30% the number of metastatic lung nodules, as compared to untreated mice (Figure 8), thus supporting the concept that the drug may be particularly active in preventing melanoma invasion and metastasis.

DISCUSSION

The ability of cancer cells to migrate, invade, and metastasize to other organs represents the most lethal aspect of melanoma, as well as the major hurdle to successful therapeutic intervention.

In the present study, we demonstrated that subtoxic concentrations of MC3181 are effective in reducing the invasiveness of both two BRAF-V600D-mutated melanoma cell lines (namely, WM115 and WM266.4) as well as of the BRAF-V600E-mutated human melanoma cell line SK-MEL-5.

We previously reported [6] the high antiproliferative activity of MC3181 against a wide panel of melanoma cells *in vitro*. Here, we confirmed this potent and concentration-dependent ability in both 2D monolayer and 3D multicellular spheroids cultures. Moreover, since cell adhesion is a fundamental step involved in the physiological processes of proliferation, invasion, as well as the pathology of neoplastic transformation and metastasis, we were prompted to investigate the capacity of MC3181 to hinder this phenomenon in both 2D and 3D-cultures. The drug successfully affected the adhesion properties of cell cultures, and interfered also with invadopodia formation. Moreover, MC3181 caused a concentration-dependent decrease of lactate levels in the high glycolytic WM266.4 cells. MC3181 acted selectively to inhibit lactate formation without affecting intracellular metabolites involved in glucose, phospholipid and energetic metabolism of this cell line. Indeed, an increase in intracellular lactate (Warburg metabolic phenotype) causes a consistent acidification of the tumor microenvironment triggering epithelial–mesenchymal transition (EMT) in melanoma cells and promoting invasion and metastasis through expression, activation and secretion of proteolytic enzymes [13]. Consequently, the ability of MC3181 to counteract the formation of an acidic microenvironment may represent a crucial step in the suppression of metastatic phenotype of WM266.4 cells. Overall, these data are paralleled by the *in vivo* antimetastatic activity observed against the highly metastatic B16-F10 murine melanoma cells.

To gain insight into the mechanisms of action underlying these results, we investigated the effects of MC3181 on the expression of genes involved in melanoma progression and metastatization, at both mRNA and protein levels. In particular, we focused our analysis on the transcription factor AP2, known to regulate the developmental choice between growth and differentiation in several embryonic tissues, and whose expression

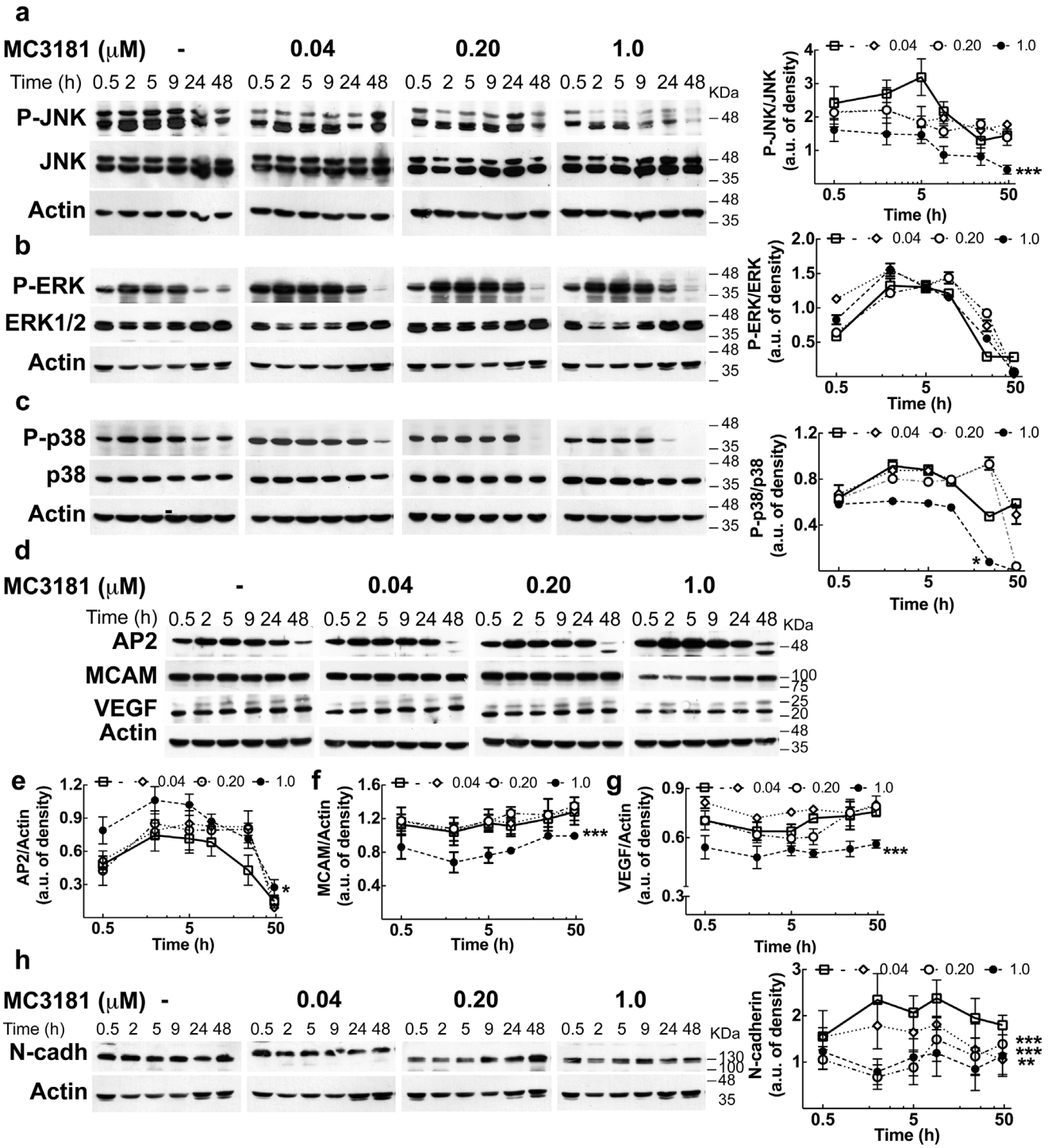

Figure 7: MC3181 causes a persistent decrease of JNK/p38 phospho-activation and of the expression of proteins involved in melanoma invasion. Immunoblot and densitometric analysis of **a.** P-JNK, **b.** P-ERK, **c.** P-p38 in absence (-□-) and in presence of MC3181 0.04 μM (-◊-), 0.20 μM (-○-) and 1.0 μM (-●-). The data revealed a significant decrease of P-JNK after only 30 minutes treatment with 1.0 μM MC3181 (***P < 0.0005 *vs* control). A sustained decrease of the phospho-active form of p38 was also observed at the highest MC3181 concentration (1.0 μM, *P < 0.05 *vs* control). Immunoblot of **d.** AP-2, MCAM/MUC18 (CD146) and VEGF. Actin was used as loading control. Densitometric analysis revealed a prolonged (up to 24 hours) increase of **e.** AP2 expression after treatment with 1.0 μM MC3181 (*P < 0.05 *vs* control) that paralleled the persistent decrease of the expression levels of **f.** MCAM/MUC18 and **g.** VEGF (***P < 0.0005 *vs* control) caused by 1.0 μM MC3181. All subtoxic concentrations of MC3181 (from 0.04 to 1.0 μM) were also able to efficiently reduce the **h.** N-cadherin expression up to 48 hours in WM266.4 cells (**P < 0.005 and ***P < 0.0005 *vs* control). Phosphorylated and non-phosphorylated proteins levels were quantitated by densitometry and normalized to their respective β-actin bands; data, presented as arbitrary units, represent means ± SD of three independent experiments. The x-axis is in logarithmic scale.

levels inversely correlate with melanoma progression in human primary melanoma specimens [14–21]. Of note, MC3181 caused an early increase in the expression levels of AP2 in the metastatic cell line, together with a decrease of N-cadherin, MCAM/MUC18 and VEGF. In fact, this transcription factor acts as a tumor suppressor, and its loss results in the up-regulation of the expression of several genes involved in the acquisition of the metastatic phenotype [16, 22–24].

In particular, N-cadherin favors the interaction of melanoma cells with other cell types expressing N-cadherin, such as fibroblasts or vascular endothelial cells [25, 26], thus fostering the access of tumor cells to the vasculature and the formation of metastases [27]. This process is also promoted by the proteolytic activity of matrix metalloproteinase MMP-2, which degrades collagen IV [28], a major constituent of ECM, and favors melanoma cells to cross the basal lamina and migrate to their secondary sites of growth. Indeed, we showed here that MC3181 also induced a significant reduction of MMP-2 activity. These data are also supported by the evidence that MC3181 treatment decreases the number of cells with active invadopodia. Thus, MC3181 treatment appears to force melanoma towards a less aggressive phenotype lowering the expression of several proteins involved in invasion and angiogenesis.

We previously reported that cytotoxic amounts of NBDHEX and MC3181 can disrupt the interaction between GSTP1-1 and TRAF2, leading to a prolonged activation of different MAPK pathways and eventually cell death [6, 29]. This is in contrast with the fact that activation of MAPKs is involved in the control of cell migration and invasion by regulating the expression and activation of MMPs [30]; in particular, the activating mutations in the Ras/Raf/MEK/ERK proteins result in constitutive signaling that promote the oncogenic behavior of melanomas. Moreover, the MAP kinase JNK plays a role in the acquisition of the metastatic phenotype, acting at multiple levels. JNK interacts with and phosphorylates paxillin leading to an increased formation of invadopodia in gliomas [31], and JNK inhibition in melanoma by α-solanine significantly reduces cell migration and invasion [32]. Surprisingly, we found that subtoxic amounts of MC3181 not only did not activate ERK but also caused a significant and sustained decrease of the phospho-active forms of JNK and p38. This event occurred in the very early phase of drug treatment, and paralleled the increase in the AP2 expression. Nonetheless, the potential involvement of alternative MC3181 targets cannot be ruled out. However, when the amount of MC3181 was increased to concentrations higher than its IC_{50} value, we confirmed the previously reported evidence

Group	Treatment (oral)	Dose	Median (range) of lung metastasis
Treated	MC3181	8 mg/kg	100 (81-107)
Control	PBS		150 (117-198)

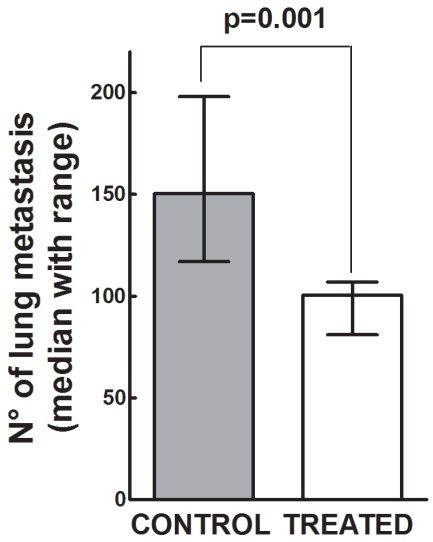

Figure 8: Antimetastatic effect of MC3181 *in vivo*. On day 0, C57BL/6 mice were injected i.v. with 1×10^5 Syngeneic B16-F10 melanoma cells. Eight hours later, they were randomly assigned to an experimental group (n = 6) and received orally MC3181 dissolved in PBS. Control group received PBS only. Mice were sacrificed on day 14, and lung metastatic nodules counted with the aid of a dissecting microscope. P = 0.001.

of a persistent phospho-activation of JNK driving cell death.

The molecular alterations reported above may also explain the effect of MC3181 treatment on the amount of lactate present in the metastatic WM266.4 cancer cells. Gao et al. [33] found higher nuclear levels of pyruvate kinase isoform M2 (PKM2) in WM266.4 cells, as compared to those recorded in the parent WM115 cells. Nuclear PKM2 could act as a coactivator of β-catenin to induce the expression of c-Myc, which in turn promotes the expression of glycolytic genes. In particular, c-Myc transcriptionally induces the expression of both glucose transporter 1 and lactate dehydrogenase A, which are required for glucose uptake and conversion of pyruvate to lactate, respectively [34]. c-Myc transcription is also regulated by the JNK/AP1 pathway [35], and the inhibition of this pathway causes a decrease in the lactate production [36]. Furthermore, the transcription factor AP-2 directly interacts with c-Myc and inhibits its binding to DNA [37]. Therefore, we may hypothesize that both inhibition of JNK phospho-activation and increment of AP2 levels may be responsible for the decrease of lactate production in WM266.4 cells upon treatment with MC3181.

Overall, the results of the present study are particularly relevant considering the high unmet need for more effective and safer systemic therapies for metastatic melanoma.

MATERIALS AND METHODS

Drugs

NBDHEX and MC3181 were synthesized as previously reported [6, 38]. For *in vitro* studies, NBDHEX, MC3181, temozolomide (TMZ; Sigma-Aldrich, Milan, Italy) and vemurafenib (VMF; Selleckem, Munich, Germany) were dissolved in DMSO. Before use, each compound was diluted to the appropriate concentration in complete culture medium; the final DMSO concentration never exceeded 0.05% (v/v). For *in vivo* studies, MC3181 was dissolved in phosphate-buffered saline (PBS).

Cell culture and treatment

The human melanoma cell lines WM115, WM266.4, SK-MEL-5, M10, and M14; the Ehlers-Danlos syndrome (EDS) derived fibroblast cell line; and the mouse melanoma cell line B16-F10 were obtained from the American Type Culture Collection (ATCC, Manassas, VA). WM115, WM266.4, M10, and M14 cell line were cultured in RPMI-1640 (EuroClone, Milan, Italy) whilst SK-MEL-5 were cultured in DMEM/F12 (Sigma-Aldrich) supplemented with 10% fetal bovine serum (FBS, v/v) (EuroClone), 2 mM L-glutamine, 100 U/ml penicillin and 100 mg/ml streptomycin (Lonza, Basel, Switzerland). B16-F10 cells were cultured in DMEM supplemented with the above-mentioned reagents and 50 mM β-mercaptoethanol. All cell lines were maintained at 37 °C in a 5% CO_2 humidified atmosphere.

For *in vitro* antiproliferative studies, WM115 (2.5×10^4 cells/cm^2), WM266.4 cells (1.25×10^4 cells/cm^2) and SK-MEL-5 (2.5×10^4 cells/cm^2) were seeded in 96-well plates and the IC_{50} values for each compound was then evaluated by the SRB assay as previously reported [5, 6].

The effects of MC3181 on cell growth and cell cycle were evaluated in WM115 and WM266.4 cell lines (2.5×10^4 and 1.25×10^4 cells/cm^2, respectively) seeded in 75 cm^2 flask (Corning B.V. Life Sciences, Amsterdam, Netherlands). Forty-eight hours after plating, cells were exposed to equiactive concentrations of MC3181 (0.05, 0.26 and 1.3 μM for WM115, and 0.04, 0.20 and 1.0 μM for WM266.4), harvested at different time points, counted using a Neubauer Chamber (after 1:1 dilution in Trypan Blue), and analyzed by a FACSCalibur instrument (BD Bioscence, San Jose, CA, USA). Flow cytometric data were analyzed by FlowJo 8.8.6 software (Tree Stare, Inc, Ashland, OR, USA).

Cell adhesion assay

A 48-well plate was coated with 200 μL of collagen (7.5 μg/ml), gelatin (0.1%), or Matrigel (0.2 mg/ml), and incubated for 2 hours at room temperature (RT). After PBS washes, plates were blocked by incubation for 30 minutes at 37°C in cell culture medium. Human melanoma cells (5×10^4 cell/well) were suspended in complete medium in the absence or presence of graded concentrations of MC3181, then plated onto the pre-coated wells, and allowed to adhere to the different substrates for 30 minutes at 37°C. Non-adhering cells were washed off with PBS, and the adhering cells were fixed with cold methanol (Sigma-Aldrich) and stained with 0.5% crystal violet. Digital photos of 3 random fields were taken at magnification 20X (3X digital camera) with an inverted microscope (Nikon ECLIPSE TS100). After imaging, the absorbance of the solubilized dye (in 100% methanol) was measured at 580 nm. The data are expressed as the mean percentages ± SD from at least three independent experiments.

Gelatin zymography

WM115 and WM266.4 cells (2×10^6) were treated with different amounts of MC3181 (0.05, 0.26 and 1.3 μM for WM115, and 0.04, 0.20 and 1.0 μM for WM266.4) for 9, 24 or 48 hours, and then lysed in Lysis Buffer [25 mM Tris-HCl (pH 7.5), 100 mM NaCl, 1% Nonidet-P-40, 1 mM PMSF, pH 7.5] (Sigma-Aldrich, Milan, Italy). After determination of protein concentration by the Lowry colorimetric assay, 20 μg of proteins were loaded, under non-reducing conditions, on 10% SDS-

polyacrylamide gels containing 0.1% gelatin (Serva ELECTROPHORESIS, Heidelberg, Germany). After electrophoresis, gels were incubated in the Renaturing Solution [2.5% Triton X-100 (Sigma-Aldrich)] for 30 minutes at room temperature, and then incubated in the developing buffer [50 mM Tris-HCl (pH 7.8), 200 mM NaCl, 5 mM $CaCl_2$, 0.02% Triton X-100] overnight, at 37°C. Gels were then stained with 0.5% Comassie blu R250 (Sigma-Aldrich) for 1 hour, and destained with 10% methanol and 5% acetic acid (Sigma-Aldrich). Activity was obtained by analysing the clear areas in the gels with the ImageJ software. The data are expressed as the mean percentages ± SD from three independent experiments.

Invadopodia assay and confocal laser scanning microscopy

WM115 and WM266.4 cells (2.0×10^4/cm^2) were seeded on 8-well chamber slides previously coated with Fluorescein-Gelatin following manufacturer's protocol (QCM™ Gelatin Invadopodia Assay Green, Millipore). After 5 hours incubation in absence and in presence of graded MC3181 concentrations (0.05, 0.26 and 1.3 μM for WM115, 0.04, 0.20 and 1.0 μM for WM266.4), cells were fixed with 3.7% formaldehyde, washed in PBS, permeabilized by fluorescent staining buffer (2% blocking serum and 0.25% Triton X-100 in DPBS without Ca^{2+} and Mg^{2+}), and then stained for TRITC-Phalloidin and DAPI following manufacturer's instruction. Fluorescence was detected using a Fluoview 1000 Olympus (Opera Zerbo, Milan, Italy) system equipped with an Olympus IX-81 inverted microscope. Acquisitions were performed with a 40X magnification oil immersion objective (NA 1.42, WD 0.15 mm). Cells with active invadopodia were defined as cells characterized by dot like structures. The Z-optical section series, obtained beginning from the nuclear apex and progressing down in 0.48 μM (at least 22 planes), were converted to maximum projection images to avoid subjectivity in the choice of the plane to be analysed. Gelatin degradation was visualized as darker areas on the coverslip due to proteolytic removal of the Fluorescein-Gelatin. Almost 100-150 cells/sample were analysed in merged images by the ImageJ software.

High-resolution ^{1}H-NMR analyses of cell extracts

WM115 (2.5×10^4 cells/cm^2) and WM266.4 cells (1.25×10^4 cells/cm^2) were plated in 150 cm^2 flasks and, 48 hours after seeding, were treated with equiactive MC3181 concentrations (0.26 and 1.3 μM for WM115, 0.20 and 1.0 μM for WM266.4). Cells were trypsinized 48 hours after treatment, counted, and assessed for viability and membrane integrity by trypan blue staining. Following washes with ice-cold PBS, cell pellets were resuspended in 0.5 ml of ice-cold twice-distilled water. Aqueous extracts (from 10 x 10^6 cells/sample) were prepared in ethanol 70% according to an established protocol [39]. Briefly, samples were ultra-sonicated at 20 kHz by a MSE ultrasonic disintegrator Mk2 (Crawley) and centrifuged at 14000 x g for 30 min. Supernatants were lyophilized twice in a RVT 4104 Savant lyophilizer (Mildford), and the residue resuspended in 0.7 ml D2O (Sigma-Aldrich, St. Louis, MO, USA) containing 0.1 mM 3-(trimethylsilyl)-propionic-2,2,3,3-d4 acid sodium salt (TSP) as internal standard. High-resolution NMR experiments (25°C) were performed at 9.4T (Bruker AVANCE). ^{1}H-NMR spectra of cell extracts were acquired using 90° flip angle, 30 s repetition time, 32K time domain data points and 128 transients [39, 40].

RNA isolation and reverse transcriptase-polymerase chain reaction (RT-PCR)

WM115 and WM266.4 cells were plated in 75cm^2 flask (2.5×10^4 cells/cm^2 and 1.25×10^4 cells/cm^2, respectively). Forty-eight hours after seeding, cells were incubated with increasing concentrations of MC3181 for 9, 24, and 48 hours. Two human melanoma cell lines (M10 and M14) were used as positive control, while the negative counterpart is represented by the Ehlers-Danlos syndrome (EDS) derived fibroblast cell line. Both control and WM115 and WM266.4 samples were detached by trypsinization, washed twice with PBS, centrifuged for 15 minutes at 1200 x g (4°C), and then frozen at -70°C in a Guanidine-Iso-Thiocyanate solution ($2x10^6$ cells/sample). RNA extraction was performed as described by Chomczyńsky and Sacchi [41], with slight modifications, and resuspended in distilled sterile water. RNA purity and concentration were determined both spectrophotometrically and electrophoretically.

For qualitative RT-PCR analysis, we designed an expression panel including different pro-angiogenic factors, cell-cell adhesion molecules, and matrix-metallo proteinases. Of note, we analyzed two out of the 6 possible transcripts of the melanoma adhesion molecule MCAM/MUC 18 gene: the short isoform, widely expressed by endothelial cells, and the long isoform, more melanoma-specific [11, 42–44]. Two micrograms of total RNA and 2.5 units of Moloney Murine Leukemia virus reverse transcriptase [45] (Applied BioSystems, Roche Molecular Systems, Inc., Branchburh, New Jersey, USA) were applied in all RT-PCR experiment, according to the manufacturer's instructions. For the generation of the first strand cDNA, the reaction mix contained 2.5 μM oligo $d(T)_{16}$, 5 mM $MgCl_2$, 1 μM dNTPs, 1 unit of RNase Inhibitor (Applied BioSystems) during 1 h incubation at 42°C. A 2μl aliquot of cDNA was used for single step PCR for all genes, with the exception of MCAM/MUC 18 that included subsequent nested PCR. Primer sequences and PCR conditions are reported in detail in Supplementary Information. The resulting nested products (25 μl) were analyzed on a 1.8% agarose gel. RNA integrity was checked

electrophoretically, and quality of cDNA was controlled by amplification of housekeeping genes such as β2-microglobulin. The level of gene expression was evaluated by densitometric analysis through the ImageJ software, and normalized with the PCR product of the housekeeping β_2-microglobulin gene, coamplified in the same experiment. All RT-PCR experiments were performed in triplicate. Under these conditions, gross quantitative estimations of mRNA expression could be detected.

Generation and analysis of 3D multicellular tumor spheroids

Spheroids were generated through the liquid-overlay technique. Briefly, 100 µl/well of cell suspension at optimized densities (0.5×10^4 cells/ml for WM115 and 0.5×10^3 for WM266.4), were dispensed onto 96-well flat-bottomed plates (Corning B.V. Life Sciences), pre-coated with 1.5% agarose (wt/vol, Serva ELECTROPHORESIS) and incubated 4 days at 37°C, in a 5% CO_2 humidified atmosphere. Spheroids treatment was performed by adding MC3181 and NBDHEX at a final concentration ranging from 0.005 to 50 µM (final incubation volume, 200 µl). Fifty percent of the medium in each well was replenished 48 hours after treatment and at day, 4, 6, 10 and 14. Spheroid size was measured up to 17 days by phase contrast imaging (10X magnification, 3X digital magnification) using a Nikon ECLIPSE TS100 inverted microscope (Nikon Instruments S.p.A, Florence, Italy), equipped with a digital camera. Images were analyzed by the ImageJ software. The radius of each tumor spheroid was used to calculate the volume (μm^3):

Eq. (1) $$V = 4/3\ \pi\ r^3$$

Spheroid growth is expressed as percentage of the volume measured in the control spheroid at the beginning of the treatment (day 0). Values are reported as means ± SD of three separate experiments, each performed in quadruplicate.

MTS assays were performed using the CellTiter Aqueous OneSolution kit (Promega Milan, Italy) according to the manufacturer's instructions. Spheroids viability is expressed as percentage of the absorbance measured in the control cells. Results are presented as means ± SD of three separate experiments, each performed in quadruplicate.

Migration and invasion assay of 2D monolayer cultures and 3D multicellular tumor spheroids

Cell migration was performed using Boyden chambers with an 8.0 µm pore size (Corning). WM266.4, WM115 (5×10^4 cell/well) and SK-MEL-5 cells (7.5×10^4 cell/well) were suspended in FBS-free media and loaded into the upper chamber, in the absence or presence of increasing MC3181 concentrations. The lower chamber was filled with complete medium supplemented with 20% FBS. For the invasion assay, the transwell membranes were previously coated with 5 µg of Matrigel (BD Biosciences, Milan, Italy). After 48-hour incubation (37°C; 5% CO_2), cells adherent to the underside of the filters were fixed and permeabilized with 70% ethanol, washed with PBS, stained with 0.25% crystal violet (Serva ELECTROPHORESIS), and counted. Four random fields at magnification 20X (3X digital camera) were counted. Percent invasion and invasion index were calculated using the following equations:

Eq. (2) $$\%\,Invasion = \frac{Mean\ of\ cells\ invading\ through\ Matrigel\ coated\ insert\ membrane}{Mean\ of\ cells\ migrating\ through\ control\ insert\ membrane}\ X\ 100$$

Eq. (3) $$\text{Invasion Index} = \frac{\%\ \text{Invasion test cells}}{\%\ \text{Invasion control cells}}$$

Results represent the means ± SD of three independent experiments.

In the spheroid invasion assay, tumor spheroids of about 330 µm diameter were transferred in a 96-well U-bottomed plate and embedded in 0.5 mg/ml of type I collagen. After collagen solidification, 100 µl of culture medium was added to the top. When present, MC3181 (0.04-1 µM) was added to both the type I collagen and the overlaid medium. Images were captured with the inverted microscope Nikon ECLIPSE TS100 after 24 and 48 hours MC3181 incubation and analyzed through the ImageJ software. Values are expressed as means ± SD of two independent experiments, each performed in quintuplicate.

Western blot analysis

At different time points after treatment, WM115 and WM266.4 cells were harvested, washed in PBS and suspended in lysis buffer containing 50 mM Tris–HCl (pH 7.4), 1 mM EDTA, 1 mM EGTA, 1% Triton X-100, 10 mM NaF, 1 mM Na_3VO_4, and protease inhibitors (Sigma–Aldrich). After 30 minutes incubation on ice, the samples were centrifuged at 13.000×g for 20 min (4°C), after which the protein concentration of the supernatant was determined using the Lowry colorimetric assay. Proteins (50 µg) were separated on 12% SDS-polyacrylamide gel and transferred onto an Immobilon-PVDF Transfer Membrane (Millipore, Billerica, MA). For immunodetection, the following primary antibodies were used: anti-phospho-JNK (Thr183/Tyr185) (Cell Signaling, Beverly, MA, USA), anti-JNK (Cell Signaling), anti-phospho-ERK1&2 (Tyr185/187; Invitrogen, Camarillo, CA), anti-ERK1&2 (Santa Cruz Biotechnology, Santa Cruz, CA), anti-phospho-p38 (Thr180/Thr182; Cell Signaling), anti-p38 (Cell Signaling), anti-AP2 (OriGene, Rockville, MD, USA), anti-CD146 (OriGene), anti-

VEGF (OriGene), anti-N-cadherin (Abcam, Cambridge, UK), anti-LC3 (Novus Biologicals, Co, USA) and anti-β actin (Sigma-Aldrich) as loading control. Anti-rabbit or anti-mouse secondary antibodies (Cell Signaling) were revealed with the ECL LiteAblot Extend (EuroClone). Band intensities were measured by the ImageJ software. Data are presented as means of arbitrary units ± SD resulting from three independent experiments.

In vivo murine melanoma lung metastasis model and treatment

Procedures involving animals and their care were in conformity with Institutional Guidelines (D.L. 116/92 and subsequent implementing circulars), and experimental protocols were approved by the local Ethical Committee of Padova University (CEASA). During *in vivo* experiments, animals in all experimental groups were examined daily for a decrease in physical activity and other signs of disease or drug toxicity; severely ill animals were euthanized by carbon dioxide overdose.

Six to eight week-old male C57BL/6 (B6) inbred mice (H-2^b) were purchased from Charles River Laboratories (Calco, Italy), and housed in our Specific Pathogen Free (SPF) animal facility. B16-F10 cells were suspended in PBS and checked for viability using trypan blue staining. Only when cell viability was > 90% the cell batch was considered for injection. B16-F10 cells (1×10^5) were injected intravenously into syngeneic C57BL/6J mice, which were then divided randomly into 2 groups (6 mice/group). Eight hours later, MC3181 was dissolved in PBS and administered orally according to a q1dx6 schedule for 2 weeks at a dose of 8 mg/kg/day. Control group received PBS. Mice were then sacrificed after two weeks of treatment, lungs were harvested, rinsed in water, and fixed in Bouin's solution. Surface metastases were then counted with the aid of a dissecting microscope.

Statistical analysis

Statistical analyses have been performed using the Statistical Package for the Social Sciences Windows, version 15.0 (SPSS, Chicago, Illinois, USA). Descriptive statistics consisted of the mean ± SD for parameters with gaussian distributions (Kolgomorov-Smirnov test). The equality of the variances was confirmed by the Levene's Test. ANOVA one-way followed by Dunnett's test was used for multiple comparison among treatment groups (>2) and control. A P value < 0.05 was considered statistically significant.

ACKNOWLEDGMENTS

We thank Dr. Claudia Matteucci and Dr. Ayele Argaw-Denboba for their valuable advice, the Centre for Advanced Microscopy 'Patrizia Albertano' and Dr. Elena Romano of University of Rome 'Tor Vergata' for imaging acquisition.

CONFLICTS OF INTEREST

The authors have no conflicts of interest to declare.

GRANT SUPPORT

A.M.C. was supported by a Consolidate the Foundations 2015 grant; A.D.L was supported by a fellowship from Fondazione Umberto Veronesi; D.R. was supported by AIRC-TRIDEO 2015 (Id.17515) and PRIN 2012 (prot. 2012CTAYSY) grants.

REFERENCES

1. Haier J, Nicolson GL. Tumor cell adhesion under hydrodynamic conditions of fluid flow. APMIS: acta pathologica, microbiologica, et immunologica Scandinavica. 2001; 109:241-262.
2. Chambers AF, Groom AC, MacDonald IC. Dissemination and growth of cancer cells in metastatic sites. Nature reviews Cancer. 2002; 2:563-572.
3. Nguyen DX, Bos PD, Massague J. Metastasis: from dissemination to organ-specific colonization. Nature reviews Cancer. 2009; 9:274-284.
4. Morris EJ, Jha S, Restaino CR, Dayananth P, Zhu H, Cooper A, Carr D, Deng Y, Jin W, Black S, Long B, Liu J, Dinunzio E, Windsor W, Zhang R, Zhao S, et al. Discovery of a novel ERK inhibitor with activity in models of acquired resistance to BRAF and MEK inhibitors. Cancer Discov. 2013; 3:742-750.
5. Graziani G, Artuso S, De Luca A, Muzi A, Rotili D, Scimeca M, Atzori MG, Ceci C, Mai A, Leonetti C, Levati L, Bonanno E, Tentori L, Caccuri AM. A new water soluble MAPK activator exerts antitumor activity in melanoma cells resistant to the BRAF inhibitor vemurafenib. Biochemical pharmacology. 2015; 95:16-27.
6. De Luca A, Rotili D, Carpanese D, Lenoci A, Calderan L, Scimeca M, Mai A, Bonanno E, Rosato A, Geroni C, Quintieri L, Caccuri AM. A novel orally active water-soluble inhibitor of human glutathione transferase exerts a potent and selective antitumor activity against human melanoma xenografts. Oncotarget. 2015; 6:4126-4143. doi: 10.18632/oncotarget.2798.
7. Smalley KS, Lioni M, Noma K, Haass NK, Herlyn M. *In vitro* three-dimensional tumor microenvironment models for anticancer drug discovery. Expert opinion on drug discovery. 2008; 3:1-10.
8. Chan GK, Kleinheinz TL, Peterson D, Moffat JG. A simple high-content cell cycle assay reveals frequent discrepancies between cell number and ATP and MTS proliferation assays. PloS one. 2013; 8:e63583.

9. Davis GE. Affinity of integrins for damaged extracellular matrix: alpha v beta 3 binds to denatured collagen type I through RGD sites. Biochemical and biophysical research communications. 1992; 182:1025-1031.
10. Kleinman HK, Martin GR. Matrigel: basement membrane matrix with biological activity. Seminars in cancer biology. 2005; 15:378-386.
11. Capoluongo E, Paolillo C, Vendittelli F. Is quantitative real time polymerase chain reaction MCAM transcript assay really suitable for prognostic and predictive management of melanoma patients? The British journal of dermatology. 2014; 171:190-191.
12. Mowers EE, Sharifi MN, Macleod KF. Autophagy in cancer metastasis. Oncogene. 2016.
13. Bohme I, Bosserhoff AK. Acidic tumor microenvironment in human melanoma. Pigment Cell Melanoma Res. 2016.
14. Bar-Eli M. Molecular mechanisms of melanoma metastasis. Journal of cellular physiology. 1997; 173:275-278.
15. Karjalainen JM, Kellokoski JK, Eskelinen MJ, Alhava EM, Kosma VM. Downregulation of transcription factor AP-2 predicts poor survival in stage I cutaneous malignant melanoma. Journal of clinical oncology. 1998; 16:3584-3591.
16. Jean D, Gershenwald JE, Huang S, Luca M, Hudson MJ, Tainsky MA, Bar-Eli M. Loss of AP-2 results in up-regulation of MCAM/MUC18 and an increase in tumor growth and metastasis of human melanoma cells. The Journal of biological chemistry. 1998; 273:16501-16508.
17. Huang S, Jean D, Luca M, Tainsky MA, Bar-Eli M. Loss of AP-2 results in downregulation of c-KIT and enhancement of melanoma tumorigenicity and metastasis. The EMBO journal. 1998; 17:4358-4369.
18. Bar-Eli M. Role of AP-2 in tumor growth and metastasis of human melanoma. Cancer metastasis reviews. 1999; 18:377-385.
19. Karjalainen JM, Kellokoski JK, Mannermaa AJ, Kujala HE, Moisio KI, Mitchell PJ, Eskelinen MJ, Alhava EM, Kosma VM. Failure in post-transcriptional processing is a possible inactivation mechanism of AP-2alpha in cutaneous melanoma. British journal of cancer. 2000; 82:2015-2021.
20. Nyormoi O, Bar-Eli M. Transcriptional regulation of metastasis-related genes in human melanoma. Clinical & experimental metastasis. 2003; 20:251-263.
21. Orso F, Penna E, Cimino D, Astanina E, Maione F, Valdembri D, Giraudo E, Serini G, Sismondi P, De Bortoli M, Taverna D. AP-2alpha and AP-2gamma regulate tumor progression via specific genetic programs. FASEB journal. 2008; 22:2702-2714.
22. Gershenwald JE, Sumner W, Calderone T, Wang Z, Huang S, Bar-Eli M. Dominant-negative transcription factor AP-2 augments SB-2 melanoma tumor growth *in vivo*. Oncogene. 2001; 20:3363-3375.
23. West-Mays JA, Sivak JM, Papagiotas SS, Kim J, Nottoli T, Williams T, Fini ME. Positive influence of AP-2alpha transcription factor on cadherin gene expression and differentiation of the ocular surface. Differentiation; research in biological diversity. 2003; 71:206-216.
24. Ruiz M, Pettaway C, Song R, Stoeltzing O, Ellis L, Bar-Eli M. Activator protein 2alpha inhibits tumorigenicity and represses vascular endothelial growth factor transcription in prostate cancer cells. Cancer research. 2004; 64:631-638.
25. Salomon D, Ayalon O, Patel-King R, Hynes RO, Geiger B. Extrajunctional distribution of N-cadherin in cultured human endothelial cells. Journal of cell science. 1992; 102:7-17.
26. Navarro P, Ruco L, Dejana E. Differential localization of VE- and N-cadherins in human endothelial cells: VE-cadherin competes with N-cadherin for junctional localization. The Journal of cell biology. 1998; 140:1475-1484.
27. Li G, Satyamoorthy K, Herlyn M. N-cadherin-mediated intercellular interactions promote survival and migration of melanoma cells. Cancer research. 2001; 61:3819-3825.
28. Sternlicht MD, Werb Z. How matrix metalloproteinases regulate cell behavior. Annual review of cell and developmental biology. 2001; 17:463-516.
29. Sau A, Filomeni G, Pezzola S, D'Aguanno S, Tregno FP, Urbani A, Serra M, Pasello M, Picci P, Federici G, Caccuri AM. Targeting GSTP1-1 induces JNK activation and leads to apoptosis in cisplatin-sensitive and -resistant human osteosarcoma cell lines. Mol Biosyst. 2012; 8:994-1006.
30. Yang M, Huang CZ. Mitogen-activated protein kinase signaling pathway and invasion and metastasis of gastric cancer. World journal of gastroenterology. 2015; 21:11673-11679.
31. Ueno H, Tomiyama A, Yamaguchi H, Uekita T, Shirakihara T, Nakashima K, Otani N, Wada K, Sakai R, Arai H, Mori K. Augmentation of invadopodia formation in temozolomide-resistant or adopted glioma is regulated by c-Jun terminal kinase-paxillin axis. Biochemical and biophysical research communications. 2015; 468:240-247.
32. Lu MK, Shih YW, Chang Chien TT, Fang LH, Huang HC, Chen PS. alpha-Solanine inhibits human melanoma cell migration and invasion by reducing matrix metalloproteinase-2/9 activities. Biological & pharmaceutical bulletin. 2010; 33:1685-1691.
33. Gao X, Wang H, Yang JJ, Liu X, Liu ZR. Pyruvate kinase M2 regulates gene transcription by acting as a protein kinase. Mol Cell. 2012; 45:598-609.
34. Yang W, Zheng Y, Xia Y, Ji H, Chen X, Guo F, Lyssiotis CA, Aldape K, Cantley LC, Lu Z. ERK1/2-dependent phosphorylation and nuclear translocation of PKM2 promotes the Warburg effect. Nat Cell Biol. 2012; 14:1295-1304.
35. Vartanian R, Masri J, Martin J, Cloninger C, Holmes B, Artinian N, Funk A, Ruegg T, Gera J. AP-1 regulates cyclin D1 and c-MYC transcription in an AKT-dependent manner

in response to mTOR inhibition: role of AIP4/Itch-mediated JUNB degradation. Mol Cancer Res. 2011; 9:115-130.

36. Park H, Jeoung NH. Inflammation increases pyruvate dehydrogenase kinase 4 (PDK4) expression via the Jun N-Terminal Kinase (JNK) pathway in C2C12 cells. Biochem. Biophys. Res. Commun. 2016; 469:1049-1054.
37. Gaubatz S, Imhof A, Dosch R, Werner O, Mitchell P, Buettner R, Eilers M. Transcriptional activation by Myc is under negative control by the transcription factor AP-2. EMBO J. 1995; 14:1508-1519.
38. Ricci G, De Maria F, Antonini G, Turella P, Bullo A, Stella L, Filomeni G, Federici G, Caccuri AM. 7-Nitro-2,1,3-benzoxadiazole derivatives, a new class of suicide inhibitors for glutathione S-transferases. Mechanism of action of potential anticancer drugs. The Journal of biological chemistry. 2005; 280:26397-26405.
39. Iorio E, Ricci A, Bagnoli M, Pisanu ME, Castellano G, Di Vito M, Venturini E, Glunde K, Bhujwalla ZM, Mezzanzanica D, Canevari S, Podo F. Activation of phosphatidylcholine cycle enzymes in human epithelial ovarian cancer cells. Cancer research. 2010; 70:2126-2135.
40. Iorio E, Mezzanzanica D, Alberti P, Spadaro F, Ramoni C, D'Ascenzo S, Millimaggi D, Pavan A, Dolo V, Canevari S, Podo F. Alterations of choline phospholipid metabolism in ovarian tumor progression. Cancer research. 2005; 65:9369-9376.
41. Chomczynski P, Sacchi N. Single-step method of RNA isolation by acid guanidinium thiocyanate-phenol-chloroform extraction. Analytical biochemistry. 1987; 162:156-159.
42. Alais S, Allioli N, Pujades C, Duband JL, Vainio O, Imhof BA, Dunon D. HEMCAM/CD146 downregulates cell surface expression of beta1 integrins. Journal of cell science. 2001; 114:1847-1859.
43. Rapanotti MC, Bianchi L, Ricozzi I, Campione E, Pierantozzi A, Orlandi A, Chimenti S, Federici G, Bernardini S. Melanoma-associated markers expression in blood: MUC-18 is associated with advanced stages in melanoma patients. The British journal of dermatology. 2009; 160:338-344.
44. Rapanotti MC, Suarez Viguria TM, Costanza G, Ricozzi I, Pierantozzi A, Di Stefani A, Campione E, Bernardini S, Chimenti S, Orlandi A, Bianchi L. Sequential molecular analysis of circulating MCAM/MUC18 expression: a promising disease biomarker related to clinical outcome in melanoma. Archives of dermatological research. 2014; 306:527-537.
45. Hagen RM, Rhodes A, Oxley J, Ladomery MR. A M-MLV reverse transcriptase with reduced RNaseH activity allows greater sensitivity of gene expression detection in formalin fixed and paraffin embedded prostate cancer samples. Exp Mol Pathol. 2013; 95:98-104.